Journal of Lasers in Medical Sciences

J Lasers Med Sci 2024;15:e65

Original Article

http://journals.sbmu.ac.ir/jlms

doi 10.34172/jlms.2024.65

Diode Laser-Based Photoacoustic Imaging for the Features of Benign and Malignant Uterine Tumors

Rima Walhikmah[1], Nurul Sa'adah[1], Fikhri Astina Tasmara[1], Rini Widyaningrum[2], Hanggoro Tri Rinonce[3,4], Mitrayana[1*]

[1]Department of Physics, Faculty of Mathematics and Natural Sciences, Universitas Gadjah Mada. Sekip Utara, Bulaksumur, Yogyakarta, Indonesia
[2]Department of Dentomaxillofacial Radiology, Faculty of Dentistry, Universitas Gadjah Mada. Jl. Denta, Sekip Utara, Yogyakarta, Indonesia
[3]Department of Anatomical Pathology, Faculty of Medicine, Public Health and Nursing, Universitas Gadjah Mada. Jl. Farmako, Sekip Utara, Yogyakarta, Indonesia
[4]Dr Sardjito Hospital, Sleman, Yogyakarta, Indonesia

***Correspondence to**
Mitrayana,
Email: mitrayana@ugm.ac.id

Received: August 25, 2024
Accepted: November 4, 2024
ePublished: December 23, 2024

Abstract

Introduction: Photoacoustic imaging (PAI) uses nonionizing radiation for tumor features and thus can be used as an alternative method for medical features without inducing biological effects. The study aimed to characterize a PAI system utilizing a 650-nm diode laser to detect pathological conditions (benign and malignant tumors) in human uterine tissue, including healthy tissue. The benign tumor tissue used is a leiomyoma, which is a benign tumor that occurs in the middle layer of the uterine (myometrium). Meanwhile, the malignant tumor tissue used is a type of endometrial carcinoma, which is a malignant tumor that occurs in the inner layer of the uterine (endometrium).

Methods: The human uterine tissue was obtained from the hysterectomy procedure conducted to determine the histopathological diagnosis. The PAI system uses a condenser microphone as the acoustic signal detector and a diode laser as the radiation source.

Results: The characterization results of the PAI based on a diode laser with a wavelength of 650 nm and power of 250 mW showed an optimal performance for human uterine tissue in a laser modulation frequency of 16500 Hz and a duty cycle of 50%. Obtained photoacoustic images could differentiate between healthy uterine, leiomyoma, and endometrial carcinoma tissues, as indicated by the intensity level values in each tissue type. Healthy uterine, leiomyoma, and endometrial carcinoma tissues had intensity values of 11.87, 26.84, and 37.26 a.u, respectively. A One-way ANOVA test with Bonferroni post hoc analysis revealed a significant difference in the acoustic intensity level between the groups ($P<0.05$).

Conclusion: The resulting intensity levels indicate a direct correlation with the nature of uterine tumors. The poorer the differentiation, the higher the resulting intensity.

Keywords: Diode laser; Photoacoustic Imaging; Benign; Malignant; Uterine tumor.

Introduction

Uterine tumors affect the female reproductive organs, and delays in recognizing the disease can allow the tumor to continue growing. Tumors are classified into two types based on their characteristics: benign tumors and malignant tumors or cancer. Both benign and malignant tumors in the uterine consist of various types. One type of benign tumor and one type of malignant tumor in the uterine are leiomyoma and endometrial carcinoma. Leiomyoma is a benign tumor that develops from smooth muscle in the middle layer of uterine (myometrium) and affects approximately 20%-50% of women of reproductive age. Endometrial carcinoma, on the other hand, is a malignant tumor that develops from epithelial cells in the uterine inner lining (endometrium). Its incidence continues to increase in recent years along with a high mortality.[1,2]

The primary cause of benign tumors transforming into malignant ones is often attributed to genetic mutations in normal uterine cells. Uterine tumors often cause symptoms such as abnormal bleeding outside the menstrual cycle or post-menopause. Other clinical symptoms can range from asymptomatic to progressive and recurrent symptoms that interfere daily activities. Important factors that determine the severity of symptoms in patients with uterine tumors are the location, size, and number of leiomyoma.[3]

Epidemiologically, the number of cases of benign tumors in the uterine is often not reported, resulting in a lack of data on these benign tumors. In contrast, cases of malignant tumors (cancer) in the uterus show a significant

Please cite this article as follows: Walhikmah R, Sa'adah N, Tasmara FA, Widyaningrum R, Rinonce HT, Mitrayana. Diode laser-based photoacoustic imaging for the features of benign and malignant uterine tumors. *J Lasers Med Sci.* 2024;15:e65. doi:10.34172/jlms.2024.65.

number. The World Cancer Research Fund International states that endometrial cancer is the sixth most common cancer among women worldwide, with over 400 000 new cases annually. According to Global Burden of Cancer (GLOBOCAN) data, 417 367 new cases of endometrial cancer and 97 370 deaths caused by endometrial cancer globally were recorded in 2020.[4] In Indonesia, endometrial cancer is the second most common cancer among women after breast cancer.[5]

Medical imaging of soft tissues and tumor detection are commonly performed using ultrasound (US) and magnetic resonance imaging (MRI) modalities.[6] MRI examinations are highly sensitive in detecting tumors. In addition to avoiding ionizing radiation, MRI is effective in determining tumor size and spread.[7] Although MRI is a high-sensitivity modality, it exhibits low specificity, making it less recommended for certain cases.[8] Meanwhile, the use of US demonstrates low sensitivity and limited penetration depth. Additionally, it requires an acoustic propagation medium, which may cause patient discomfort.[9] Photoacoustic imaging (PAI) is an imaging modality that does not use ionizing radiation,[10] and it produces images with high contrast [11] and can therefore detect tumors at a specific depth.

The histopathological feature is the gold standard for diagnosing uterine tumor. However, before diagnosing uterine cancer, it is necessary to first conduct anamnesis, physical examination, and supporting examination such as imaging. Ultrasonography and MRI are supporting test that can be conducted to diagnose uterine tumors. When ultrasonography is inadequate, MRI can provide additional information about endometrial thickening. However, the cost of MRI is relatively high. Therefore, new medical devices that are more affordable and deliver real-time results are required. The PAI system can be used as an alternative tool for supplementary features. This system has attracted attention for medical diagnosis and visualization because this does not produce ionizing radiation.[12]

PAI is an imaging modality that utilizes the photoacoustic effect phenomenon to image an object via a combination of US and optical imaging.[13] The PAI system can visualize structures to determine the presence and location of disease in the human body, including its application in detecting and visualizing cancer. Additionally, this system can image objects with high resolution, can provide contrast in differentiating various endogenous and exogenous factors, and can be free from ionizing radiation. This capability supports healthcare professionals in making diagnoses, guiding biopsies and surgeries, and providing tumor imaging and therapy in the reproductive system and subsequent treatment.[8,9]

The photoacoustic effect is the main working principle of the PAI system. This phenomenon occurs when modulated laser light is directed at a sample and some of the laser energy is absorbed by the sample.[10] Each sample has different absorption coefficients, depending on the chromophores (most sensitive pigments to light stimulation) present in the sample, and the chromophores involved in energy absorption depend on the wavelength used. Oxyhemoglobin and deoxyhemoglobin are endogenous chromophores found in the uterus and absorb light at specific wavelength ranges.[7,10,11] The energy at the laser wavelength absorbed by the sample is then converted into heat energy, generating photoacoustic waves or signals. These signals are then detected by a detector placed on the tissue surface.[14] Based on the properties of the tissue, the characteristic of acoustic signals produced can distinguish between healthy and abnormal tissues.[15]

The cost-effectiveness and compact size of the diode laser are two clear benefits of using one in the PAI system. Diode laser light is coherent, monochromatic, and directional, and more importantly, it is nonionizing electromagnetic radiation. PAI systems used in cancer imaging typically employ lasers with wavelengths ranging from 532 to 1100 nm.[16] Recently, a PAI technology based on a diode laser has been developed. The atomic and nuclear physics laboratory at UGM has successfully pioneered a diode laser-based PAI system. The success of this system began with the development of a PAI system, initially applied in dentistry. This achievement was demonstrated by Widyaningrum et al for imaging oral soft tissue[17] and by Sari et al for imaging periodontal disease.[17] While substantial research on cancer imaging exists, no studies have yet explored the use of PAI systems for imaging uterine tumors. Thus, this study aimed to characterize the PAI system's ability to differentiate between normal uterine tissue, leiomyoma, and endometrial carcinoma.

Material and Methods

The PAI system utilized here is a general-purpose setup that has been modified with a specific laser wavelength and power level to optimize it for cancer detection applications. Each sample was prepared, tested, and analyzed using the PAI system, along with supporting equipment, to ensure accurate and reproducible imaging results.

Sample Collection and Preparation

Sample preparation was performed after obtaining ethical approval from the ethics committee of the Faculty of Dentistry and Dental Hospital of Universitas Gadjah Mada, Yogyakarta (28/UNI/KEP/FKG-RSGM/EC/2024). The PAI system was tested on three types of uterine tissue samples: normal tissue, leiomyoma (benign tumor), and endometrial carcinoma (malignant tumor). The samples were obtained from the Anatomical Pathology Laboratory, Faculty of Medicine, Public Health and Nursing, Universitas Gadjah Mada (UGM). Each sample

was fixed in a 10% formalin buffer solution and stored in a covered dish. All samples were uniformly cut to dimensions of $(1 \times 1 \times 0.5) \pm 0.5$ cm to ensure a flat surface before preparations. Figure 1a shows the test sample design, and Figure 1b presents the top view of the sample to be scanned using the PAI system. The cut samples were then diagnosed histopathologically on hematoxylin and eosin staining slides as the gold standard to confirm leiomyoma and endometrial carcinoma. After the study, the samples were handed over to the appropriate authorities for proper waste management.

In this study, three sample groups were employed to acquire photoacoustic images of normal uterine tissue, leiomyoma, and endometrial carcinoma. Each group contained at least three samples to ensure the reproducibility of the photoacoustic images.

PAI System Configuration and Supporting Equipment

This study employed a custom-built PAI system that included a diode laser, condenser microphone and motor stepper. Details regarding the laser parameters can be found in Table 1. The supporting tools in this study include soundcard (Behringer UCM202HD, Germany), Arduino Nano microcontroller (Gravitech, Italy), motor stepper (NEMA17, China), optical power meter (Fast Laser Tech, China), frequency generator software (LuxDelux, East Europe), bluetooth speaker (Acome, China), laptop (Asus Vivobook Flip 14 TP410UR with operating system Windows11, Taiwan), tweezers (Marwa size 15cm, Pakistan), drop pipette (PE pipe size 120 mm, Mainland China), calipers (Vernier Caliper 6" (150 mm, China)), ruler (Faber-Castell, Jerman), and plastic measuring cup (R40 pot apex 50cc, Indonesia). The design of this study can be seen in Figure 2.

PAI System Calibration and Testing

The main components of the PAI system, particularly the diode laser (CRONOS, China), condenser microphone (Behringer ECM8000, Germany), and XY stage (self-assembled in this study), underwent testing and calibration to evaluate their performance. The durability of the laser (650 nm, 250 mW) was assessed using an optical power meter to measure output power. The calibration of the condenser microphone evaluated the ability of the apparatus to produce an acoustic signal. To ensure that the condenser microphone is an effective

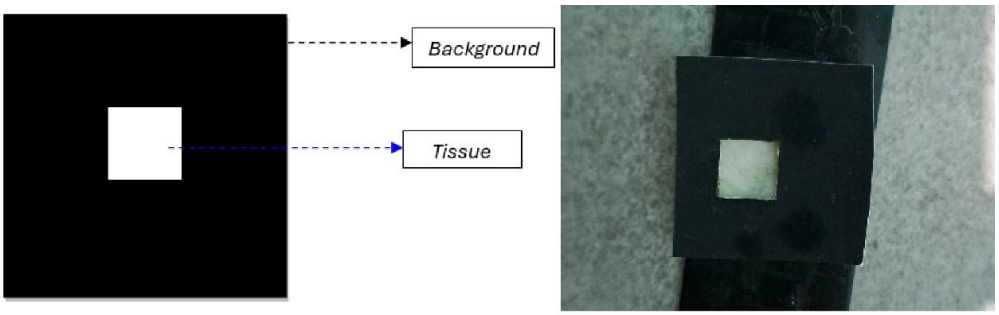

Figure 1. Tumor Sample: (a) Test Sample Design, (b) Top View of the Sample

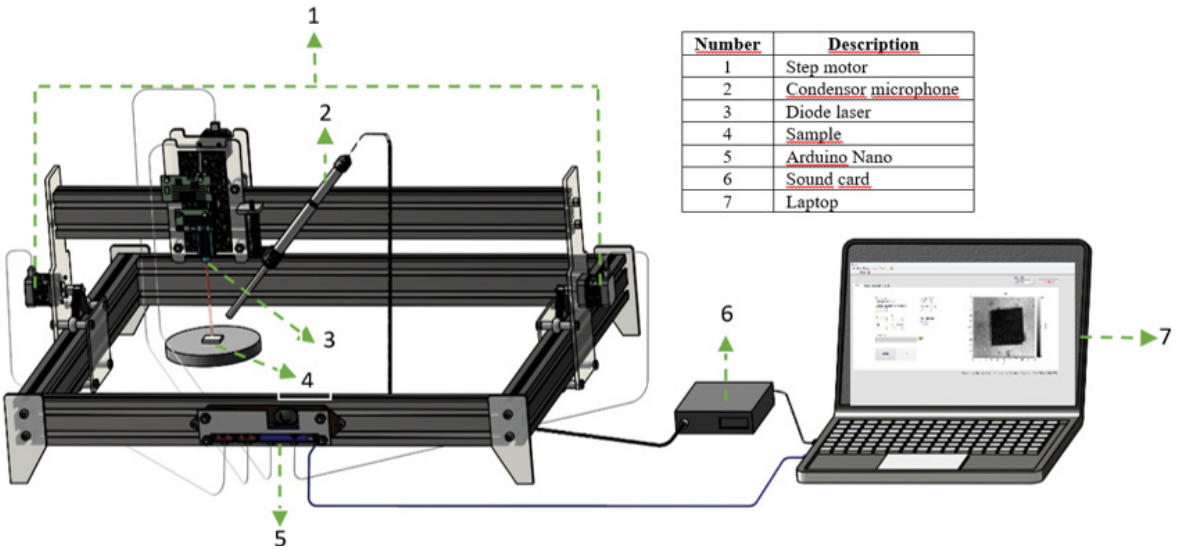

Number	Description
1	Step motor
2	Condensor microphone
3	Diode laser
4	Sample
5	Arduino Nano
6	Sound card
7	Laptop

Figure 2. Photoacoustic Imaging System

Table 1. Laser Parameters

Parameters	
Type of laser	Diode laser
Emission mode	Pulsed
Time on/time off	30.3 ms/30.3 ms (with DC 50%)
Delivery system	Directly to the sample
Energy distribution	Gaussian beam profile
Peak power	250 mW
Average power	125 mW
Spot diameter at the focus	0.1 mm
Focus spot area	7.854×10^{-5} cm^2
Spot diameter at the tissue	7.854×10^{-5} cm^2
Focus on tissue	7.854×10^{-5} cm^2
Spot area at the tissue	7.854×10^{-5} cm^2
Peak power density at spot area	7.854×10^{-5} cm^2
Peak power density at the tissue	7.854×10^{-5} cm^2
Average power density at spot area	7.854×10^{-5} cm^2
Average power density at the tissue	7.854×10^{-5} cm^2
Beam divergence	-
Water irrigation	-
Air and aspirating airflow	-

acoustic signal detector, we calibrated it by comparing the input frequency produced by the frequency generator with the output frequency detected by the microphone. By contrasting the measured displacement with the actual displacement, we also tested the XY stage to assess the accuracy of its movement in both the x and y directions.

Duty Cycle and Modulation Frequency Optimization

The optimal modulation frequency and duty cycle were tested on the samples placed on a background with holes (Figure 1b, Top view of the sample). The aim was to obtain a contrasting image that could distinguish between materials exposed to the laser. The results of the optimization obtained in the previous stage were then used to image healthy uterine, leiomyoma, and endometrial carcinoma tissues.

Image Acquisition and Analysis

Images were then analyzed using Photoacoustic Image 3.1 software available at the Atomic and Nuclear Physics Laboratory, UGM. Image reviewing included the characteristics of the cross-sectional profile of the tissue images and the average intensity level values of the images obtained from the area that included both healthy tissue and benign tumors, as well as the sample area that included the healthy tissue and malignant tumors of the uterine.

Histopathological Examination

Histopathological features were used to distinguish among normal tissue, benign tumor, and malignant tumor. Endometrial carcinoma was the malignant tumor type in this study, whereas leiomyoma was the benign tumor type. Using neutral buffered formalin 10%, we fixed tissue samples from hysterectomy specimens quickly to avoid deterioration and processed it became formalin-fixed paraffin-embedded tissues. Following sectioning, the tissue slices were put on glass slides, dewaxed, rehydrated, and then stained with hematoxylin-eosin (HE) to reveal histopathological features. Hematoxylin was used to stain the cell nuclei, followed by washing to get rid of the extra dye. To stain the cytoplasm, we subsequently submerged the slides in an eosin solution. Following dehydration, a mounting medium was used to cover the slides with glass for protection.

A pathologist performed microscopic examination to see morphological characteristic that can be used to determine the type of tumor such as altered cell sizes and shapes, increased nuclear-to-cytoplasmic ratios, and atypical tissue growth patterns. The pathologist then described all microscopic features and recorded in a histopathological report.

In this study, all samples from the three groups were imaged using a PAI system. The acoustic intensity levels from the chosen regions in each image were measured and compared between the groups. A Shapiro-Wilk test confirmed that the data followed a normal distribution. Consequently, a one-way ANOVA test with Bonferroni post hoc analysis was applied to determine whether there were statistically significant differences in acoustic intensity between the three groups. A 95% confidence level was applied to ensure the reliability of the results, enabling precise assessment of variations in acoustic signals between different sample conditions.

Results

The main components of the PAI system comprise a condenser microphone, a motor step, and a diode laser. Testing was conducted to assess the performance of the main components installed in the system.

Testing and Calibration of the Condenser Microphone

First, the condenser microphone was tested and calibrated. Before testing, calibration was performed, and the results are graphically presented in Figure 3a, showing the frequency from the function generator (v_s) and the frequency detected by the microphone (v_d). The linear fitting result ($v_d = a + bv_s$) shows a slope value of $b = 1$ and an intercept value of $a = 0$, indicating that the frequency detected by the microphone matches the frequency generated by the source. The correlation levels (adjusted R^2 and Pearson correlation) are both confirmed by the high accuracy of the microphone. These measurements confirmed that the condenser microphone

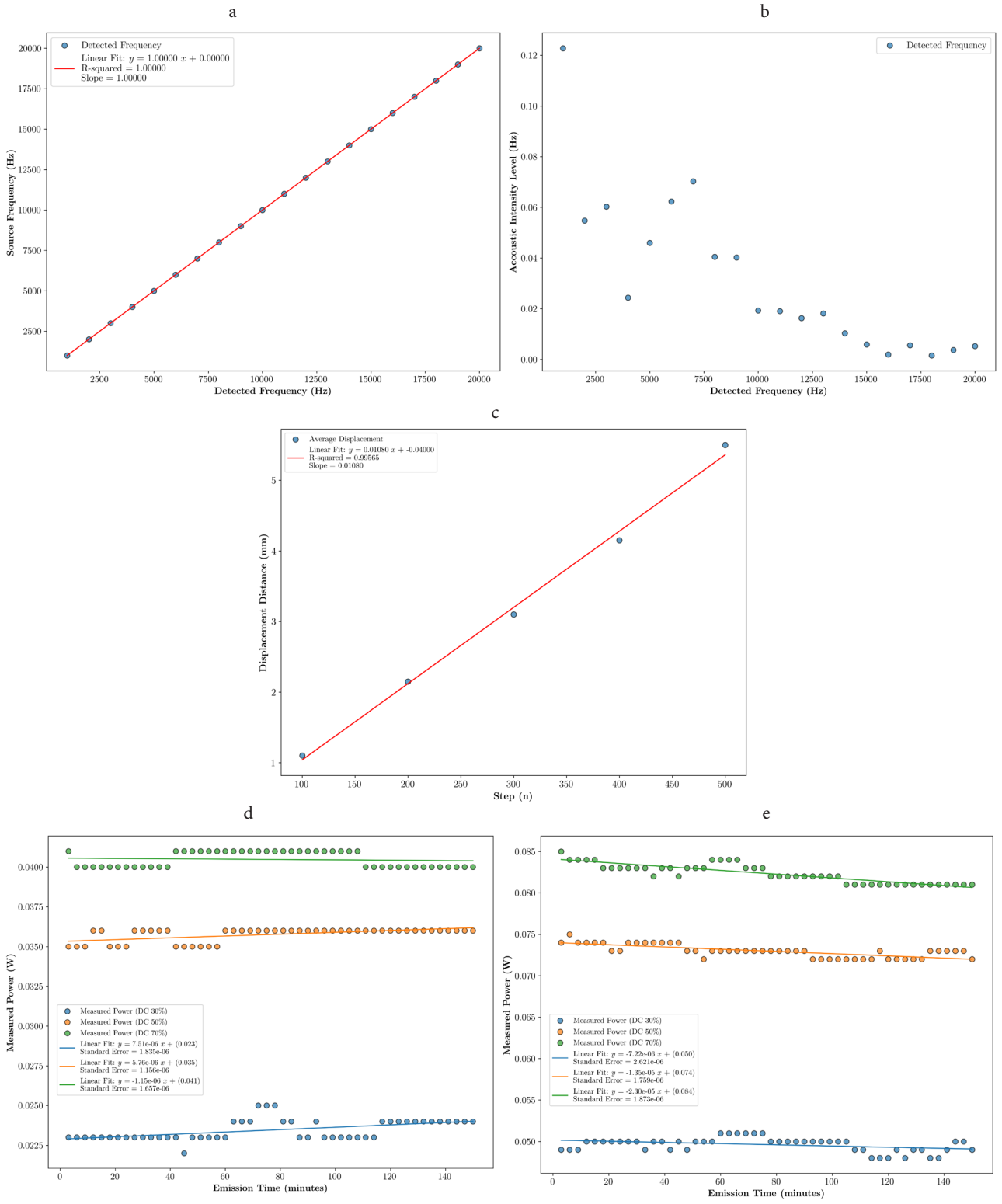

Figure 3. Calibration of the Primary Components of PAI. (a) Detected vs source frequency calibration. b) Detected frequency vs acoustic intensity level. (c) Calibration of the step motor. (d) Measured power in 10 kHz. (e) Measured power in 20 kHz

could accurately detect and distinguish input acoustic frequency parameters.

The next step involved testing the microphone by measuring the sound intensity detected against varying frequencies (from 1000 to 20 000 Hz, at 1000 Hz intervals) generated by the function generator. Data on the sensitivity of the microphone at various amplitude values for specific frequencies within the 10–20 kHz range are shown in Figure 3b. The result (Figure 3b) demonstrated microphone stability during image acquisition.

Testing and Calibration of the Stepper Motor

The step motor was also tested and calibrated to determine the displacement distance for image measurement. The displacement was obtained by dividing the measured displacement by the number of steps (see Figure 3c). The measurement results indicate that the step motor displacement was consistent and constant at 0.01 mm per step.

Testing and Calibration of Laser Power

Lastly, the laser power was tested and measured in two stages: (1) Characterization of the correlation between the duty cycle (*DC*) and laser emission power (*P*) and (2) testing the stability of measured laser emission power (*P*) over the laser-operating time. In stage (1), the input duty cycle percentages (30%, 50%, and 70%) varied with a total laser-operating time of 150 minutes. The laser emission power (*P*) was measured using the field best-optical power meter at modulation frequencies of 10 and 20 kHz. Analysis and linear fitting of the DC percentage data to the measured power (*P*) are shown in Figures 3d and 3e, indicating a correlation between the measured laser emission power and the duty cycle. Thus, the laser emission power remained stable during usage.

Optimization of the Modulation Frequency and Duty Cycle

The objective of optimizing the modulation frequency and duty cycle for the sample was to achieve optimal spatial resolution, contrast, and good image quality at an appropriate scanning speed. The correct frequency and duty cycle can help produce a good contrast between desired structures and the background or surrounding tissues. Adjusting the frequency and duty cycle can minimize noise effects in the image, thus improving the overall image quality. For imaging in uterine tissue, the optimum frequency and duty cycle obtained were 16.5 kHz and 50%, respectively. Optimization was performed with a scanning size (N_x and N_y) of 50×50 pixels and a scanning time of 0.1 seconds per step. The step (n) was set to a value of 20. The imaging area size corresponds to the background used, which has holes for the tissue samples, while the actual size of the imaged sample was not necessarily 1 cm × 1 cm, depending on the holes made in the background. The 1 cm × 1 cm size refers to the size of the resulting background and tissue sample image. The photoacoustic system was set to a size (N_x and N_y) of 50 pixels with 20 steps (n).

The results of the optimization of the frequency and optimal duty cycle obtained were used to image healthy uterine tissue, leiomyoma, and endometrial carcinoma. The PAI results for each tissue are shown in Figure 4. The intensity obtained ranged from 10 to 100 a.u. The highest intensity in the image represents the background value. As for the tissue, the lowest intensity indicates healthy tissue, while cancerous tissue shows the highest intensity. Figures 4a-4c show a photo of the tissue sample on the top, and Figures 4d-4f show a photoacoustic image on the bottom.

The intensity level of each tissue was calculated based on the graph analysis. The graphs in Figures 5d-5f at the (0,0) position indicate the background intensity value, followed by a downward trend representing the tissue intensity. The calculation of the mean acoustic intensity level, as shown by the red block, is derived solely from the tissue intensity values (excluding the background). Figure 5 shows the intensity graphs for each tissue.

Figure 5 displays the photoacoustic images generated from all study samples, along with various graphs

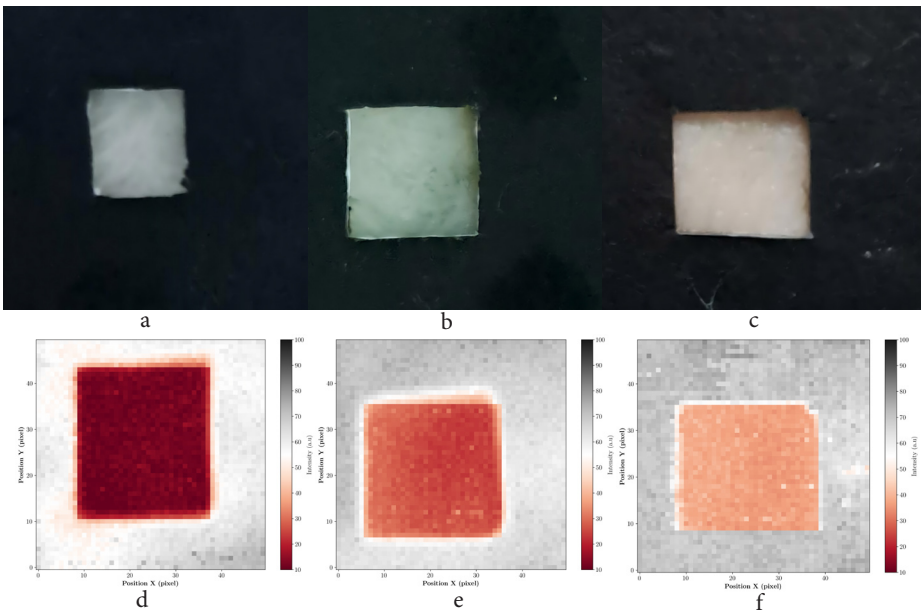

Figure 4. Visualization Results of the Tissues: (a) normal, (b) leiomyoma, (c) endometrial carcinoma, and the photoacoustic imaging results: (d) normal, (e) leiomyoma, (f) endometrial carcinoma.

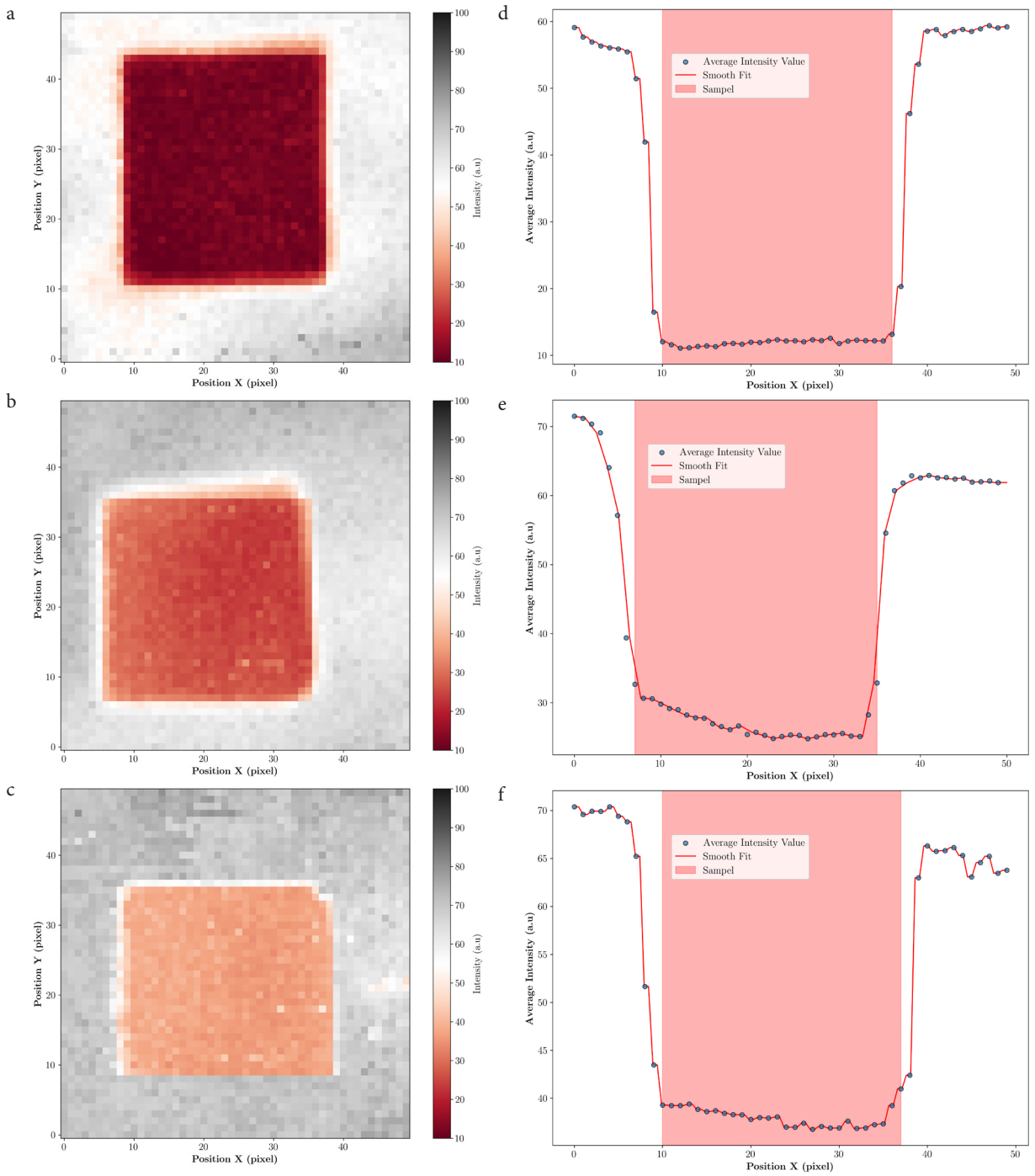

Figure 5. Photoacoustic Imaging Results: (a) normal tissue, (b) leiomyoma, (c) endometrial carcinoma, and the average intensity analysis graphs: (d) normal tissue, (e) leiomyoma, and (f) endometrial carcinoma.

depicting the average intensity analysis across samples of healthy tissue, leiomyoma, and endometrial carcinoma. The analysis results of the graph in the photoacoustic images, the mean acoustic intensity levels, of the samples are presented in Table 2 to facilitate the reading of the average acoustic intensity values.

Histopathological Features

Histopathological examination was conducted in this study as the gold standard for diagnosis. Figures 6a and 6b illustrate the histopathological features of leiomyoma and endometrial carcinoma, respectively. These images were captured at a magnification of 100×, allowing for detailed observation of cellular structures and organization.

Figure 6a shows classic histopathological features of leiomyoma. It was characterized by longitudinal and transverse fascicles of uniform smooth muscle cells with areas of hyalinization between them. The tumor cells

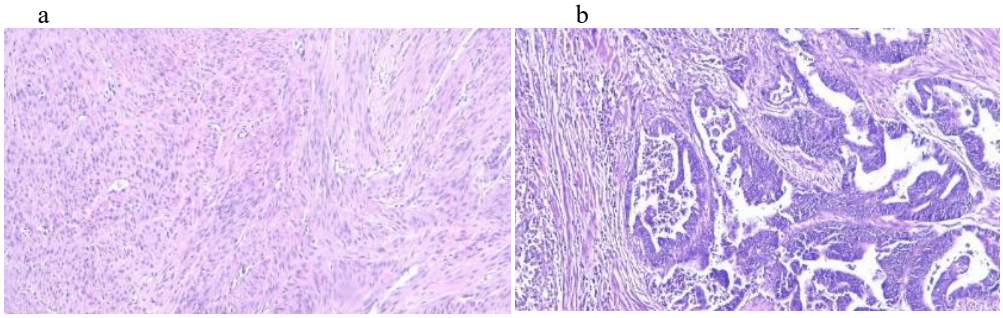

Figure 6. The histopathological features of a) leiomyoma and b) endometrial carcinoma

Table 2. Average Acoustic Intensity Levels of Uterine Tissue Samples

Sample	Total Samples	Average Acoustic Intensity (a.u)	Standard Deviation (a.u)
Healthy uterine	3	11.9	1.2
Leiomyoma	3	26.8	2.8
Endometrial Carcinoma	3	37.3	1.6

appear spindle-shaped, with eosinophilic cytoplasm and cigar shaped nuclei. No mitosis was observed. No evidence of malignancy was found.

Figure 6b shows histopathological features of endometrioid carcinoma, a type of endometrial carcinoma. Microscopically, the tumor cells were arranged in confluent or back-to-back glands lacking intervening stroma, and cribriform, infiltrating the surrounding connective tissue and muscles, extending more than half of the myometrium thickness. The tumor cells were pleomorphic, mostly columnar in shape, with scant vacuolated cytoplasm, oval nuclei, irregular nuclear membranes, coarse chromatin, and prominent nucleoli. Numerous mitoses were observed. There were haemorrhage, necrosis, and lymphocytes infiltration in the stroma.

The results of the one-way ANOVA test with Bonferroni post hoc analysis, as shown in Figure 7, indicate significant differences in acoustic intensity levels between the sample groups ($P<0.05$). Specifically, the endometrial carcinoma group exhibited the highest acoustic intensity, suggesting a strong acoustic signal response associated with malignancy. Furthermore, the leiomyoma group demonstrated higher acoustic intensity levels than the normal tissue group, although the intensity remained lower than that of the endometrial carcinoma group. These findings highlight distinct acoustic profiles among the tissue conditions, potentially showing differences in tissue structure and composition, which are imaged effectively by the PAI system.

Discussion

The PAI system operates based on the optimization of modulation frequency and optimal duty cycle. This stage can affect the imaging results and the samples used. If not

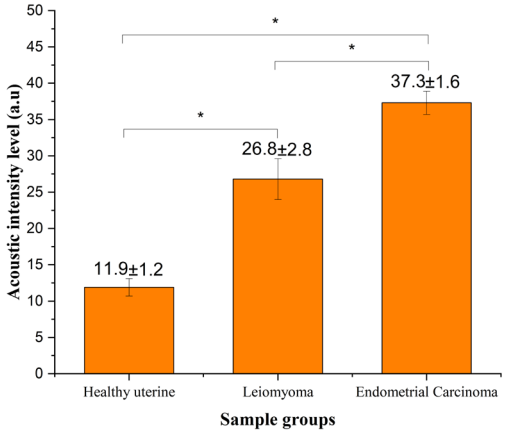

Figure 7. Mean Difference in the Acoustic Intensity Levels Between the Sample Groups. *The one-way ANOVA with the Bonferroni post hoc test is significant at $P<0.05$

correctly aligned, the samples used may be damaged or the resulting images may not provide any information. Scanning was performed on three samples: normal uterine tissue, leiomyoma (benign tumor) tissue, and endometrial carcinoma (malignant tumor) tissue. The imaging area used was 1×1 cm to ensure that the resulting images could distinguish between the background and the tissue.

The photoacoustic images of normal uterine, leiomyoma, and endometrial carcinoma tissues displayed different intensity variations per tissue type (Figure 4d-4f). The gray color in the imaging results indicates the background, while pink and dark red represent tissue images. The choice of a black background using perforated cardboard in a rectangular shape was based on the author's experiment and had not been conducted in previous studies (Figure 1). Black was chosen as this can absorb all intensities, creating a contrast with the tissue. The color gradients displayed are not the default gradients from the PAI system but are the result of processing during analysis. The PAI system provides colors in a gray-scale gradient. Coloring the imaging results facilitates the distinction between the image and the tissue. Low intensity is indicated by red, whereas high intensity is indicated by gray. The three PAI results did show significant intensity differences between each

tissue type. Endometrial carcinoma tissue has a harder, denser, and less flexible texture compared to normal uterine tissue. These textural changes indicate alterations in structure, increased collagen deposition, fibrosis, and cellular components.

Figure 4 displays the outcomes of imaging uterine tissue under various circumstances. Visually, the tissue images in each sample exhibit color differences, and they exhibit varying textures between normal tissue and tissue affected by tumor or cancer. Normal tissue tends to be softer than other tissues, and the photoacoustic system shows different intensities for each image. Normal tissue had an intensity value of (11.9 ± 1.2) arbitrary units (a.u.), leiomyoma tissue had an intensity value of (26.8 ± 2.8) a.u., and carcinoma tissue had an intensity value of (37.3 ± 1.6) a.u. The statistical analysis (Figure 7) revealed that there were significant differences between the sample groups in this study. The mean acoustic intensity level in leiomyoma has a high standard deviation, but this does not imply that the imaged tissue is carcinoma or cancerous tissue. This is because leiomyoma and endometrial carcinoma originate from different cell types. Additionally, leiomyoma is a tumor that does not have the potential to develop into cancerous cells.

The intensity differences in each tissue are also influenced by the electromagnetic absorption characteristics on the tissue surface. Biological tissues have different absorption coefficients, depending on the type of endogenous chromophores within them.[17] Endogenous chromophores are pigments or molecules found in biological tissues, such as hemoglobin, lipids, water, and melanin, being able to absorb and convert light energy into other forms of energy at specific wavelengths.[18]

The selection of the appropriate wavelength can determine the imaging results. Wavelengths between 532 and 1100 nm are absorbed by chromophores such as hemoglobin (oxy and deoxy), melanin, lipids, and water present in cancer tissues. This absorption can produce images that can differentiate between normal and cancerous tissues.[16,17] Thus, a wavelength of 650 nm can distinguish between normal and cancerous tissues. Cancerous tissues have a higher hemoglobin content than normal tissues because of the intensive formation of new blood vessels (angiogenesis). This higher content causes these tissues to absorb more light energy, increasing acoustic signals and image intensity. Thus, photoacoustic images of cancerous tissues have a higher intensity than normal tissues (as seen in Figure 3).

Formalin is a widely used fixation solution that preserves the molecular structure of tissues. However, formalin can interact with proteins and cellular structures differently in normal and tumor tissues. This interaction can cause the intensity in tumor tissues to be higher because of more prominent structural and protein changes. Additionally, cancer tissues have higher effective atomic numbers (Z_{eff}) and electron densities (ρ_{eff}), which can influence the intensity produced by the PAI system.[19]

The analysis of the average intensity in the images of normal uterine, leiomyoma, and endometrial carcinoma tissues is shown in Figure 5. The mean acoustic intensity level on each graph initially shows the value for the background, followed by a decrease in the mean intensity level, indicating the value for the tissue sample. The mean acoustic intensity level for each tissue sample is calculated by summing the intensity levels of all pixels/ data points within the tissue and dividing the sum by the total number of pixels/ data points, as indicated by the red block on the graph.

Conclusion

This study demonstrated that a PAI system using visible light at 650 nm can image uterine tissue with satisfactory results. The specifications of input parameters, including modulation frequency and duty cycle percentage, suitable for the sample used were 16.5 kHz and 50%, respectively. The system successfully distinguished tissue types through their acoustic intensity values, with normal tissue showing (11.9 ± 1.2) a.u., leiomyoma (26.8 ± 2.8) a.u., and endometrial carcinoma (37.5 ± 1.6) a.u. Statistical analysis using One-way ANOVA with Bonferroni post hoc analysis confirmed significant differences in acoustic intensity levels between the three groups ($P < 0.05$). These results suggest that higher acoustic intensity values correlate with malignant conditions, as observed in the carcinoma samples, further validating the ability of the system to differentiate between normal, benign tumor, and malignant tumor tissues.

Acknowledgments

Author would like to thank Indonesia Endowment Fund for Education (LPDP) from the Ministry of Finance Republic Indonesia for granting the scholarship and supporting this research. The authors thank Atika Windra Sari and Eka Wahyuni for their assistance during the study.

Authors' Contribution

Conceptualization: Rima Walhikmah, Rini Widyaningrum.
Data curation: Rima Walhikmah, Nurul Sa'adah, Fikhri Astina Tasmara.
Formal analysis: Rima Walhikmah, Hanggoro Tri Rinonce.
Funding acquisition: Mitrayana.
Investigation: Rima Walhikmah, Nurul Sa'adah, Fikhri Astina Tasmara.
Methodology: Rima Walhikmah, Mitrayana, Rini Widyaningrum.
Project administration: Rima Walhikmah, Nurul Sa'adah, Fikhri Astina Tasmara.
Resources: Mitrayana.
Software: Mitrayana.
Supervision: Mitrayana, Rini Widyaningrum.
Validation: Mitrayana, Rini Widyaningrum, Hanggoro Tri Rinonce.
Visualization: Rima Walhikmah.
Writing–original draft: Rima Walhikmah.
Writing–review & editing: Nurul Sa'adah, Rini Widyaningrum, Mitrayana, Hanggoro Tri Rinonce.

Competing Interests

The authors declare no conflict of interest.

Ethical Approval

The research protocol was approved by the research ethical committee of the Faculty of Dentistry and Professor Soedomo Dental Hospital, Universitas Gadjah Mada, Yogyakarta, Indonesia (Ref: 28/UNI/KEP/FKG-RSGM/EC/2024).

Funding

This publication was funded by Universitas Gadjah Mada under the *Rekognisi Tugas Akhir* (Final Project Recognition) 2024 program (No. 5286/UN1.P1/PT.01.03/2024).

References

1. Le D, Dey CB, Byun K. Imaging findings of a torsed pedunculated uterine leiomyoma: a case report. Radiol Case Rep. 2020;15(2):144-9. doi: 10.1016/j.radcr.2019.11.001.
2. Mazidimoradi A, Momenimovahed Z, Khalajinia Z, Allahqoli L, Salehiniya H, Alkatout I. The global incidence, mortality, and burden of uterine cancer in 2019 and correlation with SDI, tobacco, dietary risks, and metabolic risk factors: an ecological study. Health Sci Rep. 2024;7(1):e1835. doi: 10.1002/hsr2.1835.
3. Ghosh S, Naftalin J, Imrie R, Hoo WL. Natural history of uterine fibroids: a radiological perspective. Curr Obstet Gynecol Rep. 2018;7(3):117-21. doi: 10.1007/s13669-018-0243-5.
4. Sung H, Ferlay J, Siegel RL, Laversanne M, Soerjomataram I, Jemal A, et al. Global cancer statistics 2020: GLOBOCAN estimates of incidence and mortality worldwide for 36 cancers in 185 countries. CA Cancer J Clin. 2021;71(3):209-49. doi: 10.3322/caac.21660.
5. Brohet KE, Ramli I. Tatalaksana Radioterapi Kanker Endometrium Dengan Fokus Pada Stadium Dini. Radioter Onkol Indones. 2015;6(1):37-49. doi: 10.32532/jori.v6i1.32.
6. Aristokli N, Polycarpou I, Themistocleous SC, Sophocleous D, Mamais I. Comparison of the diagnostic performance of magnetic resonance imaging (MRI), ultrasound and mammography for detection of breast cancer based on tumor type, breast density and patient's history: a review. Radiography (Lond). 2022;28(3):848-56. doi: 10.1016/j.radi.2022.01.006.
7. Amin J, Sharif M, Yasmin M, Fernandes SL. A distinctive approach in brain tumor detection and classification using MRI. Pattern Recognit Lett. 2020;139:118-27. doi: 10.1016/j.patrec.2017.10.036.
8. Arnold TC, Freeman CW, Litt B, Stein JM. Low-field MRI: clinical promise and challenges. J Magn Reson Imaging. 2023;57(1):25-44. doi: 10.1002/jmri.28408.
9. Sari AW, Widyaningrum R, Setiawan A, Mitrayana. Photoacoustic imaging of gingival inflammation using low-cost near-infrared diode laser. Appl Acoust. 2024;218:109903. doi: 10.1016/j.apacoust.2024.109903.
10. Moore C, Cheng Y, Tjokro N, Zhang B, Kerr M, Hayati M, et al. A photoacoustic-fluorescent imaging probe for proteolytic gingipains expressed by *Porphyromonas gingivalis*. Angew Chem Int Ed Engl. 2022;61(30):e202201843. doi: 10.1002/anie.202201843.
11. Periyasamy V, Gisi K, Pramanik M. Ex vivo human teeth imaging with various photoacoustic imaging systems. Biomed Opt Express. 2024;15(9):5479-90. doi: 10.1364/boe.531436.
12. Wu Y, Zhang HK, Kang J, Boctor EM. An economic photoacoustic imaging platform using automatic laser synchronization and inverse beamforming. Ultrasonics. 2020;103:106098. doi: 10.1016/j.ultras.2020.106098.
13. Sari AW, Widyaningrum R, Yana M. Photoacoustic imaging for periodontal disease examination. J Lasers Med Sci. 2022;13:e37. doi: 10.34172/jlms.2022.37.
14. Lin L, Wang LV. The emerging role of photoacoustic imaging in clinical oncology. Nat Rev Clin Oncol. 2022;19(6):365-84. doi: 10.1038/s41571-022-00615-3.
15. Biswas D, Kumari A, Chen GC, Vasudevan S, Gupta S, Shukla S, et al. Quantitative differentiation of pneumonia from normal lungs: diagnostic assessment using photoacoustic spectral response. Appl Spectrosc. 2017;71(11):2532-7. doi: 10.1177/0003702817708320.
16. Valluru KS, Wilson KE, Willmann JK. Photoacoustic imaging in oncology: translational preclinical and early clinical experience. Radiology. 2016;280(2):332-49. doi: 10.1148/radiol.16151414.
17. Widyaningrum R, Agustina D, Mudjosemedi M, Mitrayana. Photoacoustic for oral soft tissue imaging based on intensity modulated continuous-wave diode laser. Int J Adv Sci Eng Inf Technol. 2018;8(2):622-7. doi: 10.18517/ijaseit.8.2.2383.
18. Steinberg I, Huland DM, Vermesh O, Frostig HE, Tummers WS, Gambhir SS. Photoacoustic clinical imaging. Photoacoustics. 2019;14:77-98. doi: 10.1016/j.pacs.2019.05.001.
19. Olaosun AM, Olaiya DO. Elemental characterization and radiation parameters of malignant and healthy breast tissues. J Trace Elem Miner. 2022;2:100023. doi: 10.1016/j.jtemin.2022.100023.